

Journal of Materials Chemistry A

Accepted Manuscript



This is an *Accepted Manuscript*, which has been through the Royal Society of Chemistry peer review process and has been accepted for publication.

Accepted Manuscripts are published online shortly after acceptance, before technical editing, formatting and proof reading. Using this free service, authors can make their results available to the community, in citable form, before we publish the edited article. We will replace this *Accepted Manuscript* with the edited and formatted *Advance Article* as soon as it is available.

You can find more information about *Accepted Manuscripts* in the [Information for Authors](#).

Please note that technical editing may introduce minor changes to the text and/or graphics, which may alter content. The journal's standard [Terms & Conditions](#) and the [Ethical guidelines](#) still apply. In no event shall the Royal Society of Chemistry be held responsible for any errors or omissions in this *Accepted Manuscript* or any consequences arising from the use of any information it contains.

Porous BN for hydrogen generation and storageHui Zhang^{a,b}, Chuan-Jia Tong^a, Yongsheng Zhang^c, Yan-Ning Zhang^{a,d}, Li-Min Liu^{a*}^a*Beijing Computational Science Research Center, Beijing 100084, China*^b*Normal college, Shenyang University, Shenyang 110044, China*^c*Key Laboratory of Materials Physics, Institute of Solid State Physics, Chinese Academy of Sciences, Hefei 230031, China*^d*Chengdu Green Energy and Green Manufacturing Technology R&D Center, Chengdu, Sichuan, 610207, China*Email: limin.liu@csrc.ac.cn**Abstract**

Hydrogen is a highly appealing renewable energy resource, while the hydrogen generation and storage for practical applications remain a great challenge at present. Herein, a porous monolayer boron nitride, named *p*-BN, is proposed based on first-principles calculations. Compared with the perfect *p*-BN, the band gap of *p*-BN is decreased by about 0.7 eV. Interestingly, the band gap of *p*-BN can be easily modulated, and the C-doped *p*-BN possesses a moderate 1.8 eV, which can exhibit strong adsorption in the visible light region. Additionally, *p*-BN exhibits the higher ability in hydrogen storage than *h*-BN, due to the large specific surface area. The adsorption energy of hydrogen on *p*-BN can be further improved by Li decoration. The hydrogen storage on one side of the Li-decorated *p*-BN reaches a maximum 7.5 wt%, with an adsorption energy of 160 meV. Consequently, the *p*-BN has the great potential to be utilized in both hydrogen generation and storage for practical applications.

Keywords: boron nitride, nanostructures, hydrogen storage

1. Introduction

To overcome energy shortage and environment pollution, it is crucial to develop renewable energy resources instead of fossil fuels. The abundance and environmental friendliness of hydrogen make it a highly appealing energy carrier for renewable energy. However, the existing key technical barriers in hydrogen production and storage hinder the practice application of hydrogen. Since the water-splitting for hydrogen production on the TiO₂ electrode first reported by Fujishima and Honda,¹ the development of the water-splitting with a clean, economical and environment friendly approach has become promising.^{2,3} Another serious bottleneck for the full usage of hydrogen is the lack of appropriate storage materials. So far, an efficient, economical, and safe on-board hydrogen storage approach remains a long-standing challenge.

Besides traditional bulk materials, the layered materials have received tremendous attentions owing to unusual physical properties from their three-dimension (bulk) counterparts.⁴ Two-dimensional (2D) graphene has unusual Dirac fermions due to quantum confinement^{5,6}, and 1D graphene nanoribbons exhibits strong width-dependent carrier mobility^{7,8}. Besides carbon-based materials, other 2D nanomaterials, such as *h*-BN⁹⁻¹² and layered metal dichalcogenides^{13,14} have many intrinsic advantages over their bulk structures, such as large surface area and high chemical activity, which is desired for the hydrogen production and storage.¹⁵ Many promising features, such as tunable band gaps and visible light response, have been reported for graphene nanocomposites and its analogues, such as *h*-BN, C₃N₄, and MoS₂.¹⁶⁻¹⁸ MoS₂-TiO₂ heterostructures¹⁹ show enhanced photocatalytic efficiency and give the hydrogen production rate of 1.6 mol h⁻¹g⁻¹.

The III-V compounds, especially XN (X = B, Al and Ga), are basic semiconductors for optoelectronics.²⁰ Here we focused on BN because it has a lighter weight than others, and also monolayer graphene-like BN, denoted as *h*-BN, has been fabricated experimentally^{21,22}. Nevertheless, the intrinsic *h*-BN is not a good photocatalyst due to the large band gap (experimental ~6.07 eV) and no UV light adsorption^{15,22}. Therefore, the band gap of *h*-BN needs to be greatly modulated for photocatalytic hydrogen production. On the other hand, the ionic B-N bonds in 2D BN may induce an extra dipole moment, increasing the adsorption energy of hydrogen. Both experimental²³ and theoretical studies²⁴ have shown that BN nanostructures exhibit high H₂ uptake capacity due to the strong interaction between H₂ and heteropolar B-N bonds. For example, density functional theory (DFT) calculations shows that the adsorption energy of H₂ on the BN sheet is about 90 meV, which is obviously higher than that on graphite (~60 meV)²⁵. However, the adsorption is still too weak, far away from the physisorption energy of ~0.2-0.3eV for reversible operation at or near ambient temperature. It is vital to increase the adsorption energy of 2D BN for actual applications.

In this paper, the porous BN is systematically explored by the first-principles calculations. The results suggest that the porous BN exhibits excellent structural and electronic properties in both hydrogen generation and storage. The *p*-BN exhibits a band gap of 3.98 eV, which is about 0.7 eV smaller than pristine *h*-BN. The band gap of *p*-BN can be further decreased by dopants of carbon atoms, which can become 1.8 eV with the 50 % doping into the *p*-BN. The C-doped *p*-BN possesses a moderate band gap for strong adsorption of visible light. The *p*-BN possesses a remarkably enhanced surface area compared to generic *h*-BN. Additionally, the doping of Li atom on the porous BN can further improve the hydrogen storage with an adsorption energy of 260 meV per H₂, which is about four times that of perfect *h*-BN. The maximum of hydrogen storage capacity on one side of the Li-decorated porous BN is 7.5 wt%, with an adsorption energy of 160 meV, indicating that the hydrogen storage compound could be reversible at modest H₂ (T, P) conditions. Due to the high storage capacity and good

recyclable property at ambient condition, the present Li-decorated porous BN is a potential hydrogen storage material for practical applications.

2. Computational details

In this work, all calculations were performed based on density functional theory with the Vienna Ab Initio Simulation Package (VASP)^{26,27}. Projector-augmented-wave (PAW) potentials²⁸ were used to account electron-ion interactions. The generalized gradient approximation (GGA) with the Perdew-Burke-Ernzerhof (PBE) functional²⁹ was used to treat the electron exchange correlation functional. The van der Waals (vdW) interactions were corrected by using the DFT-D2 approach³⁰.

The energy cutoff (600 eV) and $9 \times 9 \times 1$ K-meshes with the Monkhorst-Pack scheme³¹ in Brillouin zone (BZ) were set to make sure the total energy converge to within 5 meV/atom. The equilibrium geometries were fully optimized with both the lattice vectors and atom coordinates relaxed with the tolerance of less than 0.01 eV/Å on each atom. To remove spurious interactions between periodic images in the supercell model, a vacuum thickness larger than 10 Å was used. The phonon calculations were performed by using the direct approach implemented in Phonopy package³². The real-space force constants were calculated from the Hellmann-Feynman forces by introducing displacements to supercells based on finite displacement method³³. Then the dynamical matrices, phonon frequencies were obtained via the force constants.

The hydrogen adsorption energy at BN was defined as:

$$E_{\text{ads}} = -[E(X + n\text{H}_2) - E(X) - nE(\text{H}_2)] / n \quad (1)$$

where $E(X + n\text{H}_2)$ and $E(X)$ represent the total energy of the cell with and without H_2 adsorbed, n is the number of the H_2 molecules, and $E(\text{H}_2)$ is the total energy of an isolated H_2 molecule.

3. Results and discussions

3.1 The atomic structure of porous BN

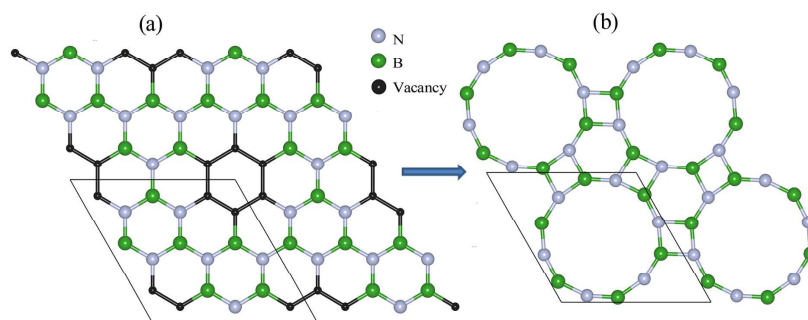


Fig. 1 The geometries of (a) original and (b) optimized porous BN (p-BN), respectively. The primitive cell is depicted by dotted lines. The gray, green, and black balls represent N, B, and vacancy atoms, respectively.

The calculated lattice parameter of the perfect *h*-BN is 2.50 Å, and the B-N bond length is 1.44 Å, in good agreement with the previous experimental and theoretical results.³⁰ A $(3 \times 3 \times 1)$ supercell of monolayer *h*-BN is used to construct a potential porous BN (*p*-BN) by

introducing vacancies, which are represented as black balls in Fig. 1(a). Interestingly, the *h*-BN with vacancies undergoes a large reconstruction after optimization. As shown in Fig. 1(b), the initial six-ring structure is nearly fully destroyed and the new structure contains a giant central porous ring with a 12-atom. The calculated lattice parameter of this new structure is 6.83 Å.

The phonon dispersion spectrum is an effective way to check whether the new *p*-BN is stable in the real situation.³⁴ The structure is stable only when all calculated frequencies are positive; otherwise, if there is any imaginary frequency, the structure should be unstable. In the phonon calculations, $6\times 6\times 1$ supercell of *h*-BN and $3\times 3\times 1$ supercell of *p*-BN were employed, respectively. The calculated phonon dispersions of *h*-BN and *p*-BN along the high-symmetry directions in the first Brillouin zone are shown in Fig. 2(a) and (b), respectively. There is no any imaginary frequency in the phonon dispersions for both structures, implying that both *h*-BN and *p*-BN are thermodynamically stable. Considering that the monolayer *h*-BN has been successfully fabricated in experiments³⁴, we may expect the fabrication of monolayer *p*-BN through generating the defect on *h*-BN in the future.

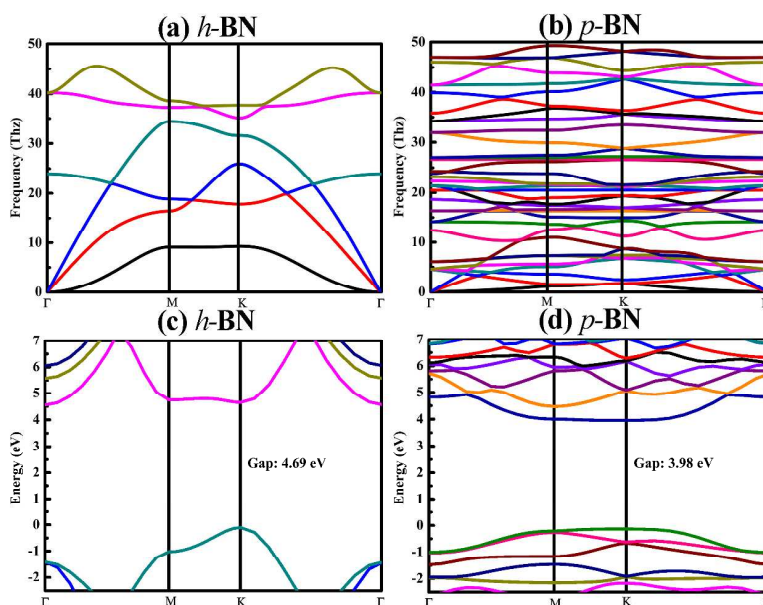


Fig. 2 The phonon dispersions of (a) *h*-BN and (b) *p*-BN, along with the electronic band structures of (c) *h*-BN and (d) *p*-BN, respectively.

3.2 Light adsorption

In order to fully utilize the solar energy, a high-performance photocatalytic material should have a band gap around 2 eV and wide adsorption range of solar energy. The electronic band structures of *h*-BN and *p*-BN are shown in Fig. 2(c) and (d). We see that the monolayer *h*-BN has a large direct band gap of 4.69 eV, and *p*-BN exhibits a relative small direct band gap of 3.98 eV. Although the band gap of *p*-BN is decreased but still too large for practical applications, which needs to narrow further for photocatalytic applications.

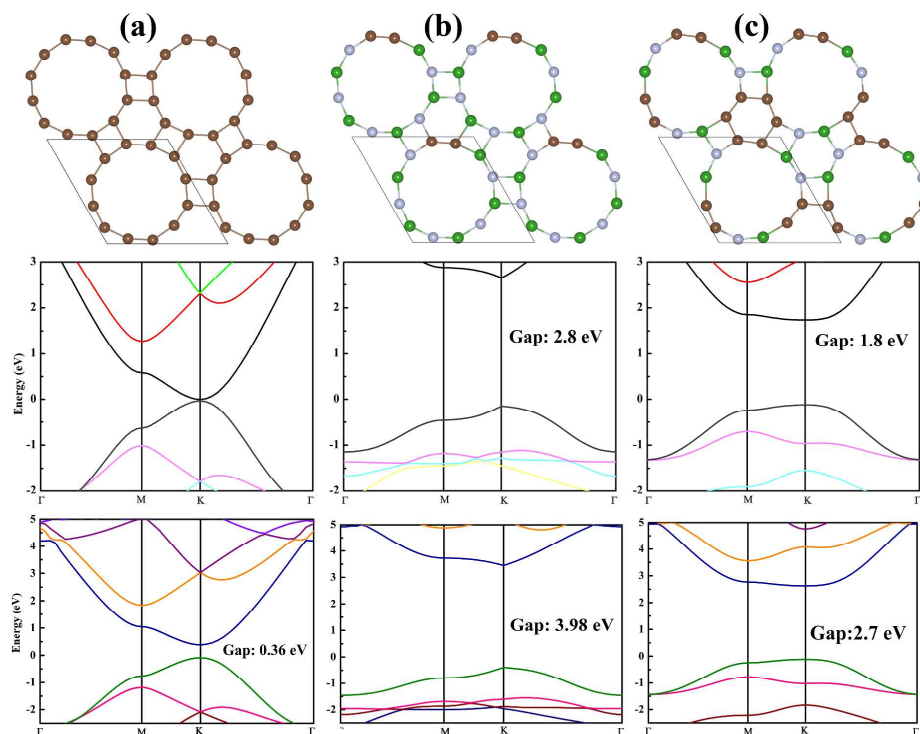


Fig. 3 The atomic configurations and electronic structures of (a) *p*-graphene and doped *p*-BN where 1/6 and 1/2 B and N atoms are replaced by C atoms in (b) and (c), respectively. The gray, green, and brown balls represent N, B, and C atoms, respectively. The middle and lower panels show the band structures calculated with PBE and HSE06, respectively.

Considering the structure similarity of graphene and *h*-BN, we first studied the electronic structure of C-based analogue of *p*-BN, which is called as *p*-graphene. As shown in Fig. 3(a), *p*-graphene has no band gap, which is exactly the same with graphene.³⁵ Therefore, we may expect a small band gap for the C-doped *p*-BN, which has been previously revealed that the band gap of *p*-BN can be further reduced by C-dopants.^{36,37} Figs. 3(b) and (c) show the optimized geometries of two C-doped *p*-BN, (denoted as *p*-CBN) where 1/6 (17 at%) and 1/2 (50 at%) of total B and N atoms are replaced by C atoms, respectively. The band structures in Fig. 3 show that the band gap is dramatically decreased to 2.8 eV for 17 at% *p*-CBN, and is 1.8 eV at 50 at% *p*-CBN. Obviously, the band gap of *p*-BN is tuneable through doping C atoms, in order to make it suitable for photocatalytic application.

It is well-known that DFT usually underestimates the band gap of semiconductor. The hybrid Heyd-Scuseria-Ernzerhof (HSE) functional and quasiparticle GW approximation can give more accurate band gap than the standard DFT.^{38,39} In the following, the typical electronic structure is further checked with the HSE06 functional. The band gap of the monolayer *h*-BN with HSE06 functional becomes 5.65 eV (see Fig. S1), which is much more reasonable than standard PBE (present 4.69 eV as shown in Fig. 2(c) and 4.56 eV in Ref⁴⁰), compared to the experimental value (6.07 eV in Ref²²). We further check the electronic structure of the pure and doped *p*-BN. Interestingly, the pure *p*-BN becomes a semiconductor with a band gap of 0.36 eV with HSE06. As for the doped *p*-BN, the band gaps become about 1 eV larger than the ones with PBE. Although the values of band gap usually change with different exchange-correlation functionals, the results arrive the same trend.

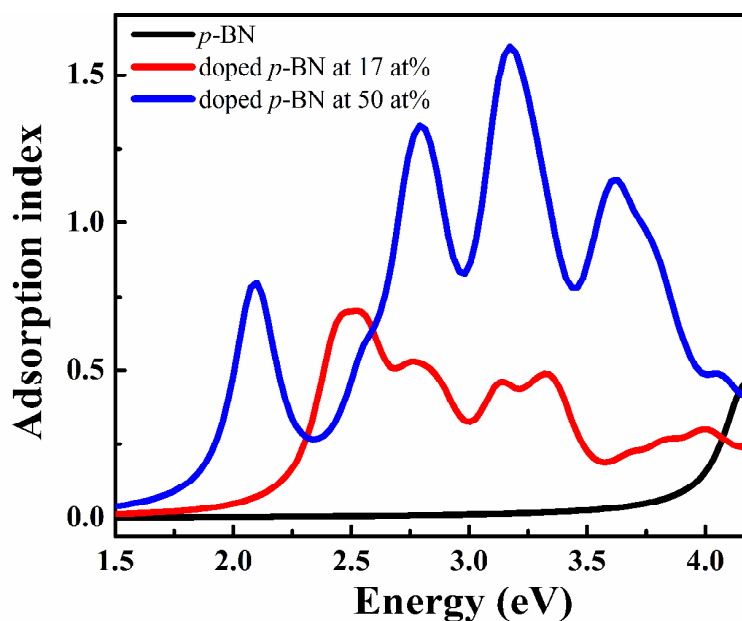


Fig. 4 Calculated optical absorption spectrum of original and C-doped *p*-BN with different constitute percentages.

One may wonder if the generic and C-doped *p*-BNs have a wide adsorption range of solar energy for photocatalytic applications. The optical absorption coefficients directly reflect the absorption range of the spectrum and are critical in solar energy conversion realm. The optical adsorption spectrum are obtained by calculating the imaginary part of the complex dielectric function⁴¹. Traditional photocatalysts, such as TiO₂, are mostly active only under ultraviolet irradiation.^{2,3} Fig. 4 clearly shows that in the visible light range (390-760 nm, 1.64-3.19 eV), the pure *p*-BN shows a negligible adsorption but the doped *p*-BNs have tremendous adsorption of solar energy. This indicates that the efficiency of solar energy utilization of *p*-BN could be largely improved by C-dopants. The optical adsorption spectrum calculated from HSE06 is shown in Fig. S2, which shows a blue-shifted light adsorption range due to larger band gap from HSE06 than from standard PBE, but also indicates that higher C-dopants lead to larger adsorption exactly the same as PBE case. Our results also stimulate the investigations on plenty of hybrid monolayers with BN structures that might possess novel electronic structures for wide applications.

3.3 Hydrogen storage

After checking the geometric stability and electronic structure of the perfect *h*-BN and porous *p*-BN, the H₂ adsorption ability was further examined. For a single H₂ adsorbed on one side of *h*-BN (0.8 wt%), the H₂ molecule sits ~3 Å above the *h*-BN layer, and the calculated adsorption energy (E_{ads}) is only 65 meV (see Fig. 5(a)). The large adsorption distance and small adsorption energy suggest the weak physisorption via vdW interactions.⁴²

With the increasing number of adsorbed H_2 , E_{ads} slightly increases with two or three H_2 adsorption, but rapidly decreases to 50 meV for 6 H_2 adsorption (5.2 wt%) due to the repulsion between neighboring H_2 (see Fig. 5(b)) Thus the maximum H_2 storage is about 2.6 wt % side of BN.

For the sole H_2 molecule adsorption on porous p -BN (1.3 wt%), its adsorption energy is 77 meV, about 18% larger than that of h -BN. The H_2 adsorption energy on p -BN decreases slightly as the number of adsorbed H_2 increases and remains around 70 meV with four H_2 molecules at p -BN (5.1 wt %, see Fig. 5(c)). The calculation results suggest that the hydrogen adsorption on h -BN should be less than 2.6 wt %, but that on p -BN can arrive at maximum 5.1 wt %.

The h -BN has a large specific surface area of 2628 m^2/g , and it can adsorb maximum 2.6 wt % hydrogen. The p -BN possesses a remarkably 24% higher specific surface area (3260 m^2/g) than h -BN. Thus, the hydrogen storage capacity (5.1 wt%) of p -BN is enlarged by about 100% compared with perfect h -BN (2.6 wt%). Nevertheless the adsorption energy at maximum hydrogen storage of these nanostructures, 65-70 meV, is too small for practical application. For the polarizable BN substrates, the H_2 storage can be enhanced by applied electric field as reported in the previous DFT calculations.⁴³ Consequently, we also expect electric field can also enhance H_2 storage capacity of present p -BN. The other approach to increase the adsorption energy is doping the nanostructures with light elements, such as calcium coating in carbon fullerenes⁴⁴ and Li-decorated porous graphene⁴⁵, both causing high capacity hydrogen storage.

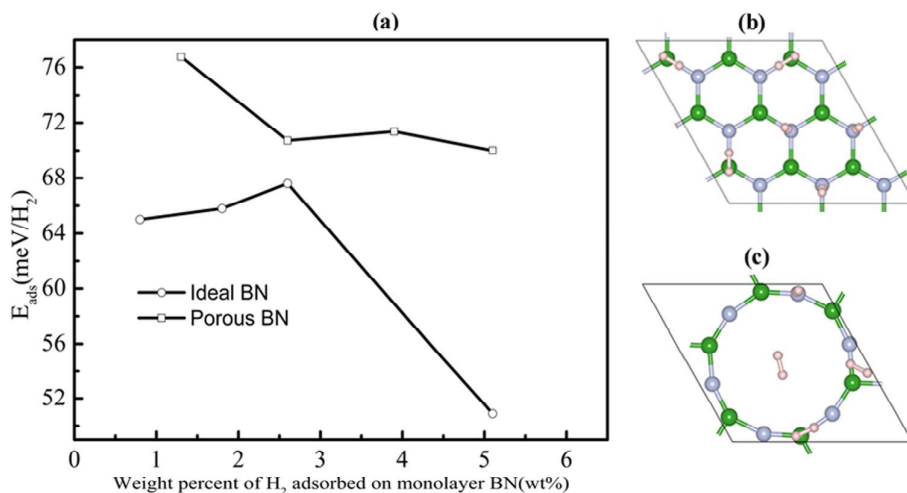


Fig. 5 (a) The adsorption energies of various structures. (b) and (c) represent the top view of geometries with maximum hydrogen adsorbed at (b) perfect BN and (c) porous BN. The gray, green, and red balls represent N, B, and H atoms, respectively.

3.4 Hydrogen storage of porous BN with Li doping

Next, we investigated whether the lithium-decoration can affect the hydrogen storage of the porous p -BN. The different configurations for the Li-decorated p -BN are considered. The adsorption energy and the optimized atomic configuration with maximum hydrogen storage are shown in Fig.6. The most stable configuration of Li-decorated p -BN is a planar structure with a lithium atom in the center of the B-N ring. H_2 tends to adsorb on Li atom, and the

adsorption energy of single H_2 is about 410 meV, which is about six times larger than that of h -BN or p -BN. One Li atom can adsorb maximum three H_2 and adsorption energy reduces to about 260 meV. The initially adsorbed Li atom lies at the center of B_6N_6 ring, but gradually approaches toward one side of BN atoms as the H_2 storage increases (see Fig. S3), which is caused by the vdW interaction between H_2 and BN atoms.

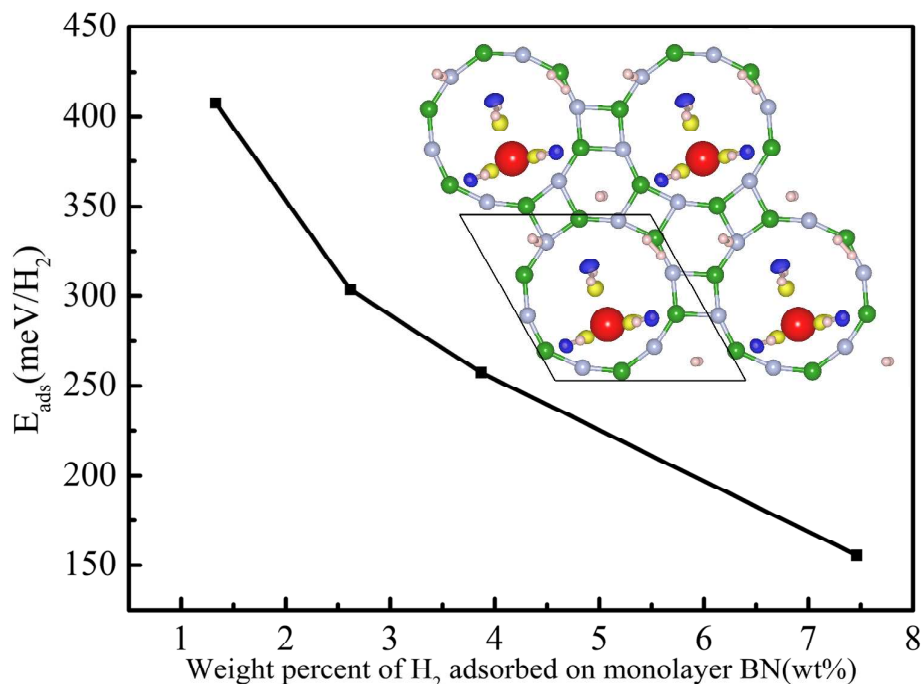


Fig. 6 The adsorption energy of hydrogen on Li-decorated p -BN and optimized geometry with maximum hydrogen storage capacity. Li atoms are represented as red balls. The charge accumulation (yellow) and depletion (blue) between Li-decorated p -BN and H_2 are also depicted with the isosurfaces of $0.04 e/\text{\AA}^3$.

The primitive cell of Li-decorated p -BN can maximally adsorb six H_2 (7.5 wt%). Three of the six H_2 molecules are adsorbed on Li atom, along with dramatic charge transfer that accounts for the high adsorption energy. The other three H_2 molecules are adsorbed far away from Li atom, exactly like the case of Li exclusion. The averaged adsorption energy of maximum capacity of p -BN is 160 meV, indicating a feasible usage in hydrogen storage at ambient pressure and temperature. As discussed above, we mainly check the hydrogen storage on one side of the Li-decorated p -BN. We also check the hydrogen storage on both sides of the Li-decorated p -BN. As shown in Fig. S4, the maximum capacity can arrive at 14 wt% with the adsorption energy of 160 meV, which is almost equal with that of one side case.

To check the consistence of different exchange correlation functional, the LDA calculations are also performed. For hydrogen adsorption on perfect h -BN, the adsorption energy is calculated to be 140 meV at 0.8 wt%, as much as twice than 65 meV of GGA value. The similar trend has been previously obtained by Jhi et al.²⁵ In the case of Li-decorated p -BN, the adsorption energy is 770 meV at 1.3 wt%, and 500 meV at 3.9 wt%. Therefore, by using different exchange-correlation functional, the values of the adsorption energies will be different, but the trend predicted here should not be changed.

In order to clarify the origin of adsorption energy, the additional calculations with pure

PBE have been performed for comparison with PBE-D case. For Li-decorated *p*-BN with 3 H₂ (3.9 wt%) and 6 H₂ (7.5 wt%), the adsorption energy is 80 meV and 14 meV, respectively, which is dramatically smaller than the one with PBE-D (260 meV and 160 meV) due to exclusion of dispersion interactions. Such a result suggests a physisorption due to vdW interaction. Additionally, in order to consider the hydrogen storage at finite temperature, we carried out ab initio molecular-dynamics calculations at T=150 K on Li-decorated *p*-BN with maximum 6 H₂ storage. After 500fs, three of H₂ remain adsorbed on Li atom but others leave the surface. Such results suggest that the Li atoms on the *p*-BN has better H₂ adsorption ability than the *p*-BN flake itself. Finally, we also calculated hydrogen adsorption on the two sides of Li-decorated *p*-BN.

4. Conclusions

The porous *p*-BN has been proposed from defective *h*-BN based on first-principles calculations. The *p*-BN not only shows thermodynamic stability, but also exhibits excellent properties in both hydrogen generation and storage. The *p*-BN exhibits a band gap of 3.98 eV, which is about 0.7 eV smaller than pristine *h*-BN. The band gap of *p*-BN can be further decreased by doping of C, which becomes 1.8 eV with the 50 % C-doping into the *p*-BN. The doped *p*-BN possesses a moderate band gap for strong adsorption in the visible light region. On the other hand, *p*-BN has larger specific surface area, which suggests higher hydrogen storage capacity than *h*-BN. The hydrogen storage of perfect *h*-BN can not exceed 2.6 wt%, but that of porous *p*-BN arrived at maximum 5.1 wt%. The Li doping *p*-BN adsorbs maximum 7.5 wt% hydrogen, and the averaged adsorption energy is 160 meV. In summary, the novel porous *p*-BN has not only an easily tuned band gap for light adsorption in the visible light region, but also higher hydrogen storage capacity.

Acknowledgments

This work was supported by the National Natural Science Foundation of China (No. 51222212), the MOST of China (973 Project, Grant NO. 2011CB922200). The computations supports from Informalization Construction Project of Chinese Academy of Sciences during the 11th Five-Year Plan Period (No.INFO-115-B01) are also highly acknowledged.

References

- 1 A. Fujishima and K. Honda, *Nature*, 1972, **238**, 37.
- 2 G. Liu, L.-C. Yin, J. Q. Wang, P. Niu, C. Zhen, Y. P. Xie and H.-M. Cheng, *Energy Environ. Sci.*, 2012, **5**, 9603.
- 3 C. H. Sun and D. J. Searles, *J. Phys. Chem. C*, 2013, **117**, 26454.
- 4 M. S. Xu, T. Liang, M. M. Shi and H. Z. Chen, *Chem. Rev.*, 2013, **113**, 3766.
- 5 K. S. Novoselov, V. I. Falko, L. Colombo, P. R. Gellert, M. G. Schwab and K. Kim, *Nature*, 2012, **490**, 192.
- 6 K. S. Novoselov, A. K. Geim, S. V. Morozov, D. Jiang, M. I. Katsnelson, I. V. Grigorieva, S. V. Dubonos and A. A. Firsov, *Nature*, 2005, **438**, 197.
- 7 Y.-W. Son, M. L. Cohen and S. G. Louie, *Phys. Rev. Lett.*, 2006, **97**, 216803.
- 8 M.-Q. Long, L. Tang, D. Wang, L. J. Wang and Z. G. Shuai, *J. Am. Chem. Soc.*, 2009, **131**, 17728.
- 9 W. Chen, Y. F. Li, G. T. Yu, C.-Z. Li, S. B. Zhang, Z. Zhou and Z. F. Chen, *J. Am. Chem. Soc.*, 2010, **132**, 1699.

- 10 S. Joshi, D. Eciija, R. Koitz, M. Iannuzzi, A. P. Seitsonen, J. Hutter, H. Sachdev, S. Vijayaraghavan, F. Bischoff, K. Seufert, J. V. Barth and W. Auwärter, *Nano Lett.*, 2012, **12**, 5821.
- 11 C. N. R. Rao, H. S. S. Ramakrishna Matte and U. Maitra, *Angew. Chem. Int. Ed*, 2013, **52**, 13162.
- 12 X. Li, X. Wu, X. C. Zeng and J. Yang, *ACS Nano*, 2012, **6**, 4104.
- 13 W. Chen, Y. F. Li, G. T. Yu, C.-Z. Li, S. B. Zhang, Z. Zhou and Z. Chen, *J. Am. Chem. Soc.*, 2010, **132**, 1699.
- 14 H. Zhang, L.-M. Liu and W.-M. Lau, *J. Mater. Chem. A*, 2013, **1**, 10821.
- 15 X. X. Li, J. Zhao and J. L. Yang, *Sci. Rep.*, 2013, **3**, 1858.
- 16 L. Britnell, R. V. Gorbachev, R. Jalil, B. D. Belle, F. Schedin, A. Mishchenko, T. Georgiou, M. I. Katsnelson, L. Eaves, S. V. Morozov, N. M. R. Peres, J. Leist, A. K. Geim, K. S. Novoselov and L. A. Ponomarenko, *Science*, 2012, **335**, 947.
- 17 A. J. Du, S. Sanvito, Z. Li, D. Wang, Y. Jiao, T. Liao, Q. Sun, Y. H. Ng, Z. Zhu, R. Amal and S. C. Smith, *J. Am. Chem. Soc.*, 2012, **134**, 4393.
- 18 X. D. Li, S. Yu, S. Wu, Y.-H. Wen, S. Zhou and Z.-Z. Zhu, *J. Phys. Chem. C*, 2013, **117**, 15347.
- 19 W. Zhou, Z. Yin, Y. Du, X. Huang, Z. Zeng, Z. Fan, H. Liu, J. Wang and H. Zhang, *Small*, 2013, **9**, 140.
- 20 H. Zhang, Y.-N. Zhang, H. Liu and L.-M. Liu, *J. Mater. Chem. A*, 2014, **2**, 15389.
- 21 L. Song, L. J. Ci, H. Lu, P. B. Sorokin, C. H. Jin, J. Ni, A. G. Kvashnin, D. G. Kvashnin, J. Lou, B. I. Yakobson and P. M. Ajayan, *Nano Lett.*, 2010, **10**, 3209.
- 22 K. K. Kim, A. Hsu, X. Jia, S. M. Kim, Y. Shi, M. Hofmann, D. Nezich, J. F. Rodriguez-Nieva, M. Dresselhaus, T. Palacios and J. Kong, *Nano Lett.*, 2011, **12**, 161.
- 23 C. Tang, Y. Bando, X. Ding, S. Qi and D. Golberg, *J. Am. Chem. Soc.*, 2002, **124**, 14550.
- 24 J. Dai, X. Wu, J. Yang and X. C. Zeng, *J. Phys. Chem. Lett.*, 2014, **5**, 393.
- 25 S.-H. Jhi and Y.-K. Kwon, *Phys. Rev. B*, 2004, **69**, 245407.
- 26 G. Kresse and J. Furthmüller, *Phys. Rev. B*, 1996, **54**, 11169.
- 27 G. Kresse and J. Furthmüller, *Comp. Mater. Sci.*, 1996, **6**, 15.
- 28 G. Kresse and D. Joubert, *Phys. Rev. B*, 1999, **59**, 1758.
- 29 J. P. Perdew, K. Burke and M. Ernzerhof, *Phys. Rev. Lett.*, 1996, **77**, 3865.
- 30 X. Wu, M. C. Vargas, S. Nayak, V. Lotrich and G. Scoles, *J. Chem. Phys.*, 2001, **115**, 8748.
- 31 H. J. Monkhorst and J. D. Pack, *Phys. Rev. B*, 1976, **13**, 5188.
- 32 A. Togo, F. Oba and I. Tanaka, *Phys. Rev. B*, 2008, **78**, 134106.
- 33 K. Parlinski, Z. Q. Li and Y. Kawazoe, *Phys. Rev. Lett.*, 1997, **78**, 4063.
- 34 Q. Li, D. Zhou, W. T. Zheng, Y. M. Ma and C. F. Chen, *Phys. Rev. Lett.*, 2013, **110**, 136403.
- 35 X. G. Luo, L.-M. Liu, Z. P. Hu, W.-H. Wang, W.-X. Song, F. F. Li, S.-J. Zhao, H. Liu, H.-T. Wang and Y. J. Tian, *J. Phys. Chem. Lett.*, 2012, **3**, 3373.
- 36 E. Perim, R. Paupitz, P. A. S. Autreto and D. S. Galvao, *J. Phys. Chem. C*, 2014, **118**, 23670.
- 37 Y. Ding, Y. L. Wang, S. Q. Shi and W. H. Tang, *J. Phys. Chem. C*, 2011, **115**, 5334.
- 38 T. Cheiwchanchamnangij and W. R. L. Lambrecht, *Phys. Rev. B*, 2012, **85**, 205302.
- 39 H. Zhang, Y.-N. Zhang, H. Liu and L.-M. Liu, *J. Mater. Chem. A*, 2014, **2**, 15389.
- 40 B. Huang and H. Lee, *Phys. Rev. B*, 2012, **86**, 245406.
- 41 R. M. Sheetz, I. Ponomareva, E. Richter, A. N. Andriotis and M. Menon, *Phys. Rev. B*, 2009, **80**, 195314.
- 42 W. Lei, H. Zhang, Y. Wu, B. Zhang, D. Liu, S. Qin, Z. Liu, L. Liu, Y. Ma and Y. Chen, *Nano Energy*, 2014, **6**, 219.

- 43 J. Zhou, Q. Wang, Q. Sun, P. Jena and X. S. Chen, *PNAS*, 2010, **107**, 2801.
- 44 M. Yoon, S. Yang, C. Hicke, E. Wang, D. Geohegan and Z. Zhang, *Phys. Rev. Lett.*, 2008, **100**, 206806.
- 45 A. Du, Z. Zhu and S. C. Smith, *J. Am. Chem. Soc.*, 2010, **132**, 2876.